Mathematical and Computational Applications

MDPI

Article

Soret & Dufour and Triple Stratification Effect on MHD Flow with Velocity Slip towards a Stretching Cylinder

Kandasamy Jagan [1] and Sivanandam Sivasankaran [2,*]

[1] Department of Mathematics, School of Engineering, Presidency University, Bangalore 560064, India; kjaganppmaths@gmail.com
[2] Department of Mathematics, King Abdulaziz University, Jeddah 21589, Saudi Arabia
* Correspondence: sd.siva@yahoo.com

Abstract: The phenomenon of convective flow with heat and mass transfer has been studied extensively due to its applications in various fields. The effects of nonlinear thermal radiation (NLTR), slip, thermal-diffusion (Soret) and diffusion-thermo (Dufour) on magenoto-hydrodynamic (MHD) flow towards a stretching cylinder in the presence of triple stratification (TSF) are investigated in this paper. The governing equations are transformed into an ODE by suitable transformations. The homotopy analysis method (HAM) is used to solve the ODE. The revamping of fluid flow, and heat transfer due to the presence of the Soret and Dufour effect, concentration slip and concentration stratification are analyzed. The temperature and local Sherwood number increases as the Dufour number rises, whereas the local Nusselt number decreases. While elevating the Soret number, the Sherwood number diminishes, whereas the concentration profile rises. The thermal boundary layer thickness enhances when thermal radiation increases. The rate of solute transport reduces while the concentration slip increases.

Keywords: radiation; slip; stratification; MHD; stretching cylinder; thermal-diffusion

Citation: Jagan, K.; Sivasankaran, S. Soret & Dufour and Triple Stratification Effect on MHD Flow with Velocity Slip towards a Stretching Cylinder. *Math. Comput. Appl.* **2022**, *27*, 25. https://doi.org/10.3390/mca27020025

Received: 24 January 2022
Accepted: 3 March 2022
Published: 9 March 2022

1. Introduction

The importance of nanofluids has been discussed before. The heat transfer in water-based nanofluids (TiO_2–H_2O, Al_2O_3–H_2O and Cu–H_2O) and thermal radiation's influence on nanofluid flow over a stretchy cylinder were studied by Rahman and Aziz [1], Rasekh et al. [2] and Pandey and Kumar [3]. The effect of thermal radiation on stagnation-point nanofluid flow towards a stretchy sheet, 3D Jeffrey fluid flow, a nanofluid flow due to a contracting cylinder, finite element simulation of MHD convective nanofluid flow in porous media and MHD flow of a casson fluid induced by a semi-infinite stretchy surface with Cattaneo–Christov heat flux were investigated by Das et al. [4], Raju et al. [5], Abbas et al. [6], Uddin et al. [7] and Sandeep et al. [8]. More recent related research was performed by Veera Krishna and Chamkha [9], Veera Krishna [10], Veera Krishna and Chamkha [11] and Animasaun et al. [12].

Concentration stratification occurs due to concentration differences, such as the inclusion of different heterogeneous mixtures. The effects of thermal stratification on flow and heat transfer and mixed convection flow due to a stretching cylinder were discussed by Chamkha et al. [13] and Mukhopadhyay and Ishak [14]. Karthikeyan et al. [15] and Eswaramoorthi et al. [16] analyzed the Soret and Dufour effect on MHD mixed convection of a stagnation point flow over a vertical plate in a porous medium with chemical reaction and viscoelastic flow, over a stretchy sheet with convective boundaries.

Hayat et al. [17] analyzed MHD nanofluid flow with double stratification and slip conditions, and concluded that temperature profile diminishes when thermal and slip stratification parameters are increased. The main aim of this paper is to analyze how the NLTR and Soret and Dufour effect play out for the mathematical model of Hayat et al. [17].

More related research was done by Faraz et al. [18], Ali et al. [19] and Abdal et al. [20]. Thus, in this paper, investigation was done on MHD flow of nanofluid towards a stretchy cylinder with thermal, nanparticle volume fraction and concentration stratification in the presence of NLTR, Soret and Dufour and slip effects. The present investigation is useful to improve the mass and heat transfer processes in thermal systems.

2. Mathematical Formulation

We consider the two-dimensional and steady Newtonian nanofluid flow towards a stretching cylinder, where the stretching cylinder is considered along z-axis and r-axis is perpendicular to it. The velocity of the stretchy cylinder is assumed as $W_w(z) = \frac{W_0 z}{l}$ where $W_0 > 0$ are constants and l is the characteristic length as shown in Figure 1. Fluid flow is considered along z-axis with slip effect and constant magnetic field. The ambient temperature, nanoparticle volume fraction and concentration are taken as $Te_\infty = Te_0 + \frac{dz}{l}$, $Cn_\infty = Cn_0 + \frac{ez}{l}$ and $S_\infty = S_0 + \frac{nz}{l}$. The fluid temperature, nanoparticle volume fraction and concentration are assumed as $Te_w = Te_0 + \frac{az}{l}$, $Cn_w = Cn_0 + \frac{bz}{l}$ and $S_w = S_0 + \frac{mz}{l}$. The following assumptions are taken:

- The flow is steady, laminar and $2D$-dimensional.
- The fluid is incompressible.
- The uniform external magnetic field is applied. The induced magnetic field is neglected.
- The cylinder is stretching with uniform velocity along z-direction.
- The stratification effect for temperature, nanoparticle volume fraction and concentration is considered.

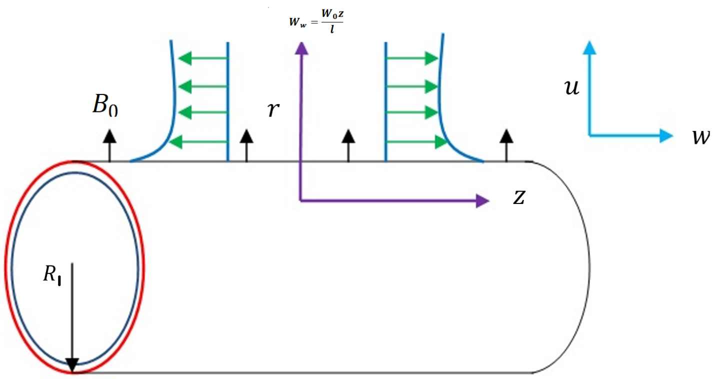

Figure 1. Physical diagram.

The thermal energy, nanoparticle volume fraction and concentration stratification effects are also considered. The governing equations for the present flow analysis (refer to Hayat et al. [17]) can be written as

Contunity Equation

$$\frac{\partial(r\,u)}{\partial r} + \frac{\partial(r\,w)}{\partial z} = 0, \tag{1}$$

Momentum Equation

$$u\frac{\partial w}{\partial r} + w\frac{\partial w}{\partial z} = \nu\left(\frac{\partial^2 w}{\partial r^2} + \frac{1}{r}\frac{\partial w}{\partial r}\right) - \frac{\sigma B_0^2}{\rho} w, \tag{2}$$

Temperature Equation

$$u\frac{\partial(Te)}{\partial r} + w\frac{\partial(Te)}{\partial z} = \alpha\left(\frac{\partial^2(Te)}{\partial r^2} + \frac{1}{r}\frac{\partial(Te)}{\partial r}\right) + \tau\left(D_B\frac{\partial(Te)}{\partial r}\frac{\partial(Cn)}{\partial r} + \frac{D_{Te}}{Te_\infty}\left(\frac{\partial(Te)}{\partial r}\right)^2\right)$$
$$-\frac{1}{(\rho c_p)}\frac{\partial q_r}{\partial r} + \frac{D_s k_T}{c_s c_p}\left(\frac{\partial^2(Cn)}{\partial r^2} + \frac{1}{r}\frac{\partial(Te)}{\partial r}\right), \tag{3}$$

Nano-Particle Volume Fraction Equation

$$u\frac{\partial(Cn)}{\partial r}+w\frac{\partial(Cn)}{\partial z}=D_B\left(\frac{\partial^2(Cn)}{\partial r^2}+\frac{1}{r}\frac{\partial(Cn)}{\partial r}\right)+\frac{D_{Te}}{Te_\infty}\left(\frac{\partial^2(Te)}{\partial r^2}+\frac{1}{r}\frac{\partial(Te)}{\partial r}\right), \quad (4)$$

Concentration Equation

$$u\frac{\partial S}{\partial r}+w\frac{\partial S}{\partial z}=D_s\left(\frac{\partial^2 S}{\partial r^2}+\frac{1}{r}\frac{\partial S}{\partial r}\right)+\frac{D_s k_T}{T_m}\left(\frac{\partial^2 T}{\partial r^2}+\frac{1}{r}\frac{\partial T}{\partial r}\right)-k_1(S-S_\infty). \quad (5)$$

where the boundary conditions are

$$\begin{aligned}
&w=W_w(z)+L\frac{\partial w}{\partial r},\ Te=Te_w(z)=k_1\frac{\partial(Te)}{\partial r},\ Cn=Cn_w(z)=k_2\frac{\partial(Cn)}{\partial r},\\
&S=S_w(z)=k_3\frac{\partial S}{\partial r}\ at\ r=R_1. \quad (6)\\
&w\to 0,\ \ Te\to Te_\infty(z),\ \ Cn\to Cn_\infty(z),\ \ S\to S_\infty(z)\ as\ r\to\infty.
\end{aligned}$$

The transformations are

$$\begin{aligned}
&\zeta=\sqrt{\frac{W_w(z)}{\nu z}}\left(\frac{r^2-R_1^2}{2R_1}\right),\ w=W_w(z)f'(\zeta),\ u=-\sqrt{\frac{\nu W_w(z)}{z}}\frac{R_1}{r}f(\zeta),\\
&\phi_1(\zeta)=\frac{Te-Te_\infty}{Te_w-Te_0},\phi_2(\zeta)=\frac{Cn-Cn_\infty}{Cn_w-Cn_0},\ s(\zeta)=\frac{S-S_\infty}{S_w-S_0}. \quad (7)
\end{aligned}$$

Equation (1) is satisfied identically, and Equations (2)–(6) are reduced to Equations (8)–(12) using Equation (7).

$$(1+2\gamma\zeta)\theta_1'''+\theta_1\theta_1''-\theta_1'^2+2\gamma\theta_1''-M^2\theta_1'=0, \quad (8)$$

$$\begin{aligned}
&(1+2\gamma\zeta)\phi_1''+2\gamma\phi_1'+(1+2\gamma\zeta)\ Pr\ Nb\ \phi_1'\phi_2'+(1+2\gamma\zeta)PrNt(\phi_1')^2\\
&+Pr(f\phi_1'-f'\phi_1-G_1f')+\frac{4}{3}\ Rd\ (1+2\gamma\zeta)\Big[(\theta_w)^3\Big(3\theta^2(\phi_1')^2+\phi_1^3\phi_1''\Big)\\
&\quad+3(\theta_w)^2\Big(2\phi_1(\phi_1')^2+\phi_1^2\phi_1''\Big)+3\theta_w\Big((\phi_1')^2+\phi_1\phi_1''\Big)+\phi_1''\Big]\\
&+\frac{4}{3}\ Rd\ \gamma\Big[\theta_w^3\phi_1^3\phi_1'+3\theta_w^2\phi_1^2\phi_1'+3\theta_w\phi_1\phi_1'+\phi_1'\Big]+D_f\big[(1+2\gamma\zeta)\phi_2''\\
&\qquad\qquad+2\gamma\phi_2'\big]=0, \quad (9)
\end{aligned}$$

$$\begin{aligned}
&(1+2\gamma\zeta)\phi_2''+2\gamma\phi_2'+Sc_n\ (\theta_1\phi_2'-\theta_1'\phi_2-G_2\theta_1')+\frac{Nt}{Nb}\big[(1+2\gamma\zeta)\phi_1''\\
&\qquad\qquad+2\gamma\phi_1'\big]=0, \quad (10)
\end{aligned}$$

$$\begin{aligned}
&(1+2\gamma\zeta)s''+2\gamma s'+Sc\ (\theta_1 s'-\theta_1' s-G_3\theta_1')+Sc\ S_r\big[(1+2\gamma\zeta)\phi_1''\\
&\qquad\qquad+2\gamma\phi_1'\big]-C_rSc\ s=0. \quad (11)
\end{aligned}$$

$$\begin{aligned}
&\theta_1(0)=0,\ \theta_1'(0)=1+A\ \theta_1''(0),\ \phi_1(0)=1-G_1-B_1\ \phi_1'(0),\\
&\phi_2(0)=1-G_2-B_2\ \phi_2'(0),\ s(0)=1-G_3-B_3\ s'(0), \quad (12)\\
&\theta_1'(\zeta)\to 0,\ \phi_1(\zeta)\to 0,\ \phi_2(\zeta)\to 0\ and\ s(\zeta)\to 0\ as\ \zeta\to\infty.
\end{aligned}$$

where

$$
\begin{aligned}
& A = L\sqrt{\frac{W_0}{\nu l}},\ B_1 = K_1\sqrt{\frac{W_0}{\nu l}},\ B_2 = K_2\sqrt{\frac{W_0}{\nu l}},\ B_3 = K_3\sqrt{\frac{W_0}{\nu l}},\ C_r = \frac{k_1 l}{W_0}, \\
& \gamma = \sqrt{\frac{\nu l}{W_0 R_1^2}},\ D_f = \frac{D_s k_T (Cn_w - Cn_0)}{\alpha c_s c_p (Te_w - Te_0)},\ G_1 = \frac{d}{a},\ G_2 = \frac{e}{b},\ G_3 = \frac{n}{m}, \\
& M^2 = \frac{\sigma l B_0^2}{\rho W_0},\ Nb = \frac{(\rho c_p)_p D_B (Cn_w - Cn_\infty)}{(\rho c_p)_f \nu}, Nt = \frac{(\rho c_p)_p D_{Te} (Te_w - Te_\infty)}{(\rho c_p)_f \nu Te_\infty}, \\
& Rd = \frac{4\sigma^* Te_\infty^3}{kk^*}, Re_z = \frac{W_0 z^2}{\nu l}, Sc = \frac{\nu}{D_s},\ Sc_n = \frac{\nu}{D_B}, S_r = \frac{D_s k_T (Te_w - Te_0)}{Te_m \nu (S_w - S_0)}, \\
& Pr = \frac{\mu c_p}{k}, \theta_w = \frac{Te_w - Te_0}{Te_\infty}.
\end{aligned} \tag{13}
$$

The skin-friction coefficient, local Nusselt and Sherwood number are given by

$$Re_z^{1/2} C_f = \theta_1''(0), \tag{14}$$

$$Re_z^{-1/2} Nu = -\left(1 + \frac{4}{3} Rd\, \theta_w^3\right)\phi_1'(0) \tag{15}$$

$$Re_z^{-1/2} Sh = -s'(0). \tag{16}$$

3. Convergence of the Solution

Equations (8)–(11) subject to Equation (12) are solved using HAM by choosing the initial boundary approximations, auxillary function and auxillary linear operators (refer to Noor et al. [21,22]) as

$$
\begin{aligned}
& \theta_{1,0}(\zeta) = \frac{1}{1+A}\left(1 - e^{-\zeta}\right),\ \phi_{1,0}(\zeta) = \left(\frac{1-G_1}{1+B_1}\right)e^{-\zeta}, \\
& \phi_{1,0}(\zeta) = \left(\frac{1-G_2}{1+B_2}\right)e^{-\zeta},\ s_0(\zeta) = \left(\frac{1-G_3}{1+B_3}\right)e^{-\zeta}.
\end{aligned} \tag{17}
$$

$$H(\zeta) = 1. \tag{18}$$

$$
\begin{aligned}
& L_{\theta_1} = \frac{d^3\theta_1}{d\zeta^3} - \frac{d\theta_1}{d\zeta},\ L_{\phi_1} = \frac{d^2\phi_1}{d\zeta^2} - \phi_1, \\
& L_{\phi_2} = \frac{d^2\phi_2}{d\zeta^2} - \phi_2,\ L_s = \frac{d^2 s}{d\zeta^2} - s,
\end{aligned} \tag{19}
$$

which satisfies the property

$$L_{\theta_1}[A_1 + A_2 * Exp(-\zeta) + A_3 * Exp(\zeta)] = 0, \tag{20}$$

$$L_{\phi_1}[A_4 * Exp(-\zeta) + A_5 * Exp(\zeta)] = 0, \tag{21}$$

$$L_{\phi_2}[A_6 * Exp(-\zeta) + A_7 * Exp(\zeta)] = 0. \tag{22}$$

$$L_s[A_8 * Exp(-\zeta) + A_9 * Exp(\zeta)] = 0. \tag{23}$$

where A_1 to A_9 are arbitrary constants. Mathematica software is used to solve the above HAM equations. The equations obtained contain the parameters $h_{\theta_1}, h_{\phi_1}, h_{\phi_2}$ and h_s. The h-curve is plotted for $M = 0.2$, $Rd = 0.1$, $Nt = 0.1$, $\theta_w = 0.1$, $Nb = 0.1$, $Pr = 1.4$, $D_f = 0.2$, $Sc_n = 1.9$, $Sc = 0.4$, $S_r = 0.2$, $\gamma = 0.1$, $C_r = 0.1$, $A = 0.1$, $G_1 = G_2 = G_3 = 0.1$ and $B_1 = B_2 = B_3 = 0.1$. The admissible ranges of $h_{\theta_1}, h_{\phi_1}, h_{\phi_2}$ and h_s are $-1.8 \leq h_{\theta_1} \leq -0.1$, $-1.3 \leq h_{\phi_1} \leq -0.1$, $-1.3 \leq h_{\phi_2} \leq -0.1$ and $-1.5 \leq h_s \leq -0.4$ (see Figure 2).

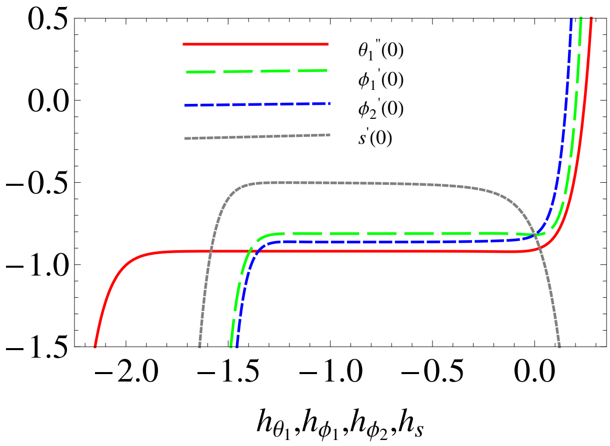

Figure 2. h-curve for $f''(0)$, $\theta'(0)$, $\phi'(0)$ and $s'(0)$.

The convergence value is tabulated in Table 1 for different orders of approximations.

Table 1. Convergence of the series $-\theta_1''(0)$, $-\phi_1'(0)$, $-\phi_2'(0)$ and $-s'(0)$ for $\gamma = 0.1$, $M = 0.2$, $Rd = 0.1$, $\theta_w = 0.1$, $Pr = 1.4$, $Nt = 0.1$, $Nb = 0.1$, $D_f = 0.2$, $Sc_n = 1.9$, $Sc = 0.4$, $C_r = 0.1$, $A = 0.1$, $S_r = 0.2$, $G_1 = G_2 = G_3 = 0.1$ and $B_1 = B_2 = B_3 = 0.1$.

m-th Order Approximation	$-\theta_1''(0)$	$-\phi_1'(0)$	$-\phi_2'(0)$	$-s'(0)$
1	0.9213	0.8190	0.8491	0.7013
4	0.9212	0.8090	0.8546	0.5695
8	0.9190	0.8101	0.8598	0.5281
12	0.9185	0.8107	0.8617	0.5147
16	0.9184	0.8110	0.8622	0.5085
18	0.9184	0.8111	0.8623	0.5066
19	0.9184	0.8112	0.8624	0.5058
20	0.9184	0.8112	0.8624	0.5051

The square residual errors are defined as follows.

$$\Delta_m^{\theta_1} = \int_0^1 \left[R_m^{\theta_1}(\zeta, h_{\theta_1})\right]^2 d\zeta, \tag{24}$$

$$\Delta_m^{\phi_1} = \int_0^1 \left[R_m^{\phi_1}(\zeta, h_{\phi_1})\right]^2 d\zeta, \tag{25}$$

$$\Delta_m^{\phi_2} = \int_0^1 \left[R_m^{\phi_2}(\zeta, h_{\phi_2})\right]^2 d\zeta, \tag{26}$$

$$\Delta_m^{s} = \int_0^1 [R_m^{s}(\zeta, h_s)]^2 d\zeta. \tag{27}$$

Equations (24)–(27) are plotted in Figure 3.

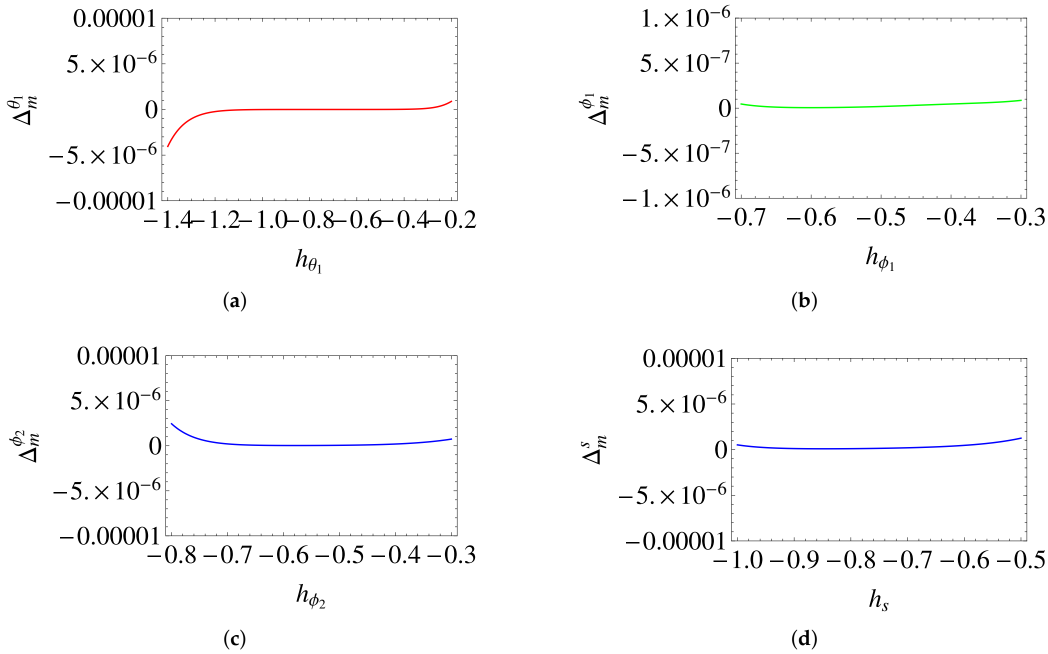

Figure 3. h-curve for the residual error (**a**) $\Delta_m^{\theta_1}$, (**b**) $\Delta_m^{\phi_1}$, (**c**) $\Delta_m^{\phi_2}$ and (**d**) Δ_m^{s}.

4. Computational Results and Discussion

Different combinations of apt parameters involved in this study are discussed. The ranges of the parameters are: $M \sim 0$ to 200 , $Rd \sim 0$ to 0.5, $Nt \sim 0.1$ to 0.5, $\theta_w \sim 0$ to 1.5, $Nb \sim 0.1$ to 0.5, $Pr \sim 1$ to 13.7, $D_f \sim 0$ to 1, $S_r \sim 0$ to 1, $\gamma \sim 0$ to 0.5, $C_r \sim 0$ to 1.5, $A \sim 0$ to 2, $G_1 \sim 0$ to 4, $G_2 \sim 0$ to 2, $G_3 \sim 0$ to 1 and $B_1 = B_2 = B_3 \sim 0$ to 1. In Tables 2 and 3, the present results of $\theta_1'(0)$ and $\theta_1''(0)$ are compared with those of Andersson [23], Mahmoud [24], Mahmoud and Waheed [25] and Hayat et al. [17] for different positive values of A. The results show good agreement.

Table 2. Comparison of $\theta_1'(0)$ for various values of A when $\gamma = M = 0$.

A	Andersson [23]	Mahmoud [24]	Mahmoud & Waheed [25]	Hayat et al. [17]	Present
0	1.0	1.0	1.0	1.0000	1.0000
0.1	0.9218	0.91279	0.91279	0.9127	0.9127
0.2	0.8447	0.84473	0.84472	0.84473	0.84473
0.5	0.7044	0.70440	0.70440	0.70440	0.70440
1.0	0.5698	0.56984	0.56982	0.56984	0.56984
2.0	0.4320	0.43204	0.43199	0.43204	0.43204
5.0	0.2758	0.27579	0.27579	0.27580	0.27580
10.0	0.1876	0.18758	0.18759	0.18781	0.18781
20.0	0.1242	0.12423	0.12420	0.12456	0.12456

Table 3. Comparison of $-\theta_1''(0)$ for various values of A when $\gamma = M = 0$.

A	Andersson [23]	Mahmoud [24]	Mahmoud & Waheed [25]	Hayat et al. [17]	Present
0	1.0	1.0	1.0	1.0000	1.0000
0.1	0.8721	0.87208	0.87209	0.872082	0.872082
0.2	0.7764	0.77637	0.77639	0.77677	0.77677
0.5	0.5912	0.59119	0.59121	0.591195	0.591159
1.0	0.4302	0.43016	0.43018	0.430159	0.430159
2.0	0.2840	0.28398	0.28400	0.283978	0.283978
5.0	0.1448	0.14484	0.14481	0.144841	0.144841
10.0	0.0812	0.08124	0.08123	0.081242	0.081242
20.0	0.0438	0.04378	0.04381	0.043772	0.043772

From Table 4, it is clear that the skin friction coefficient $\theta_1''(0)$ increases while elevating γ (>0) and M but it decreases while elevating A (>0).

Table 4. Numerical values of skin friction coefficient $\theta_1''(0)$ for different parameters.

γ	M	A	Hayat et al. [17]	Present
0.0	0.2	0.1	0.9511	0.9511
0.5			1.1007	1.1007
1.0			1.2337	1.2337
0.1	0.0		0.9021	0.9021
	0.5		1.0889	1.0889
	1.0		1.2391	1.2391
	0.2	0.0	1.1352	1.1352
		0.5	0.6554	0.6554
		1.0	0.4724	0.4724

The velocity profile is plotted for magnetic (M), curvature (γ) and velocity slip (A) parameters. From Figure 4a, it is clear that the thickness of momentum boundary layer diminishes when elevating the magnetic parameter. The physical magnetic field, along with velocity slip, develop a retarding force which controls the fluid velocity. A similar result is shown in Figure 4c because the stretching sheet cannot transmit its drag force completely to the fluid. In Figure 4b, it is shown that the thickness of momentum boundary layer rises while the curvature parameter is boosted.

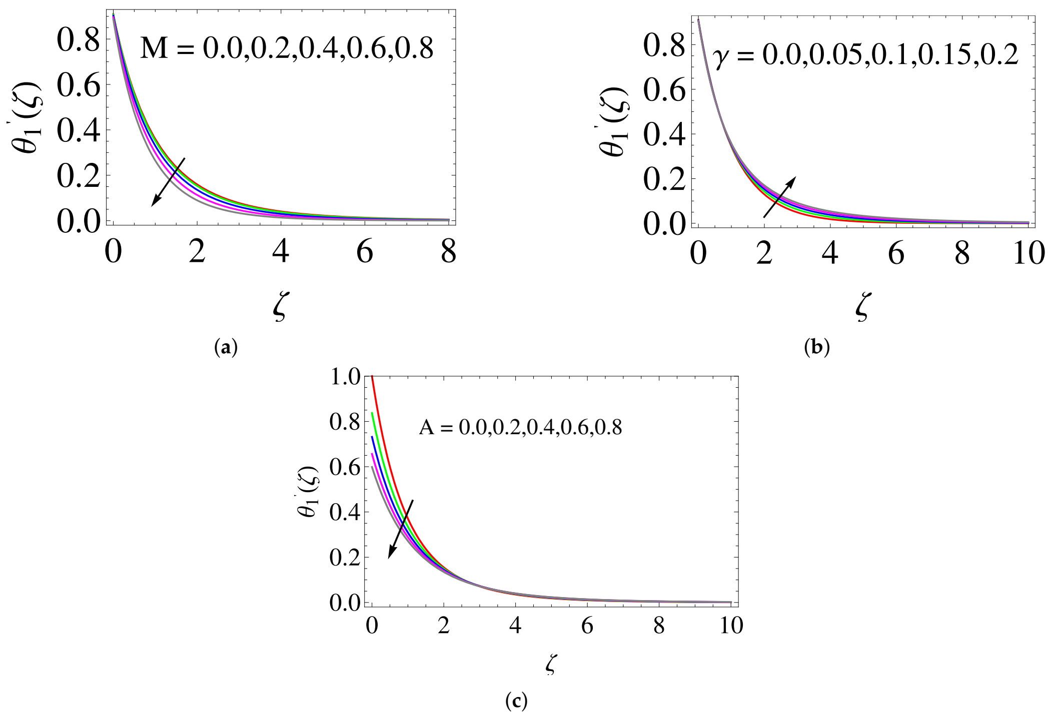

Figure 4. Influences of (**a**) magnetic (M), (**b**) curvature (γ) and (**c**) velocity slip parameters (A) on the concentration profile for $Rd = 0.1$, $Nt = 0.1$, $\theta_w = 0.1$, $Nb = 0.1$, $Pr = 1.4$, $D_f = 0.2$, $Sc_n = 1.9$, $Sc = 0.4$, $S_r = 0.2$, $C_r = 0.1$, $G_1 = G_2 = G_3 = 0.1$ and $B_1 = B_2 = B_3 = 0.1$.

Thermal boundary layer thickness increases while thermal radiation increases, as more heat is generated in the fluid (see Figure 5a). The same result is shown in Figure 5d because temperature inside the boundary layer rises. When magnetic, curvature and velocity slip parameters are boosted, thermal boundary layer thickness grows (see Figures 5b,c and 6a), but it diminishes with increases in thermal stratification, nanoparticle volume fraction stratification and thermal slip parameters (see Figure 6b–d). A physical rise in thermal stratification decreases the local bouyance level and a rise in thermal slip decreases the molecular movement of the fluid, which results in a decrease in temperature profile.

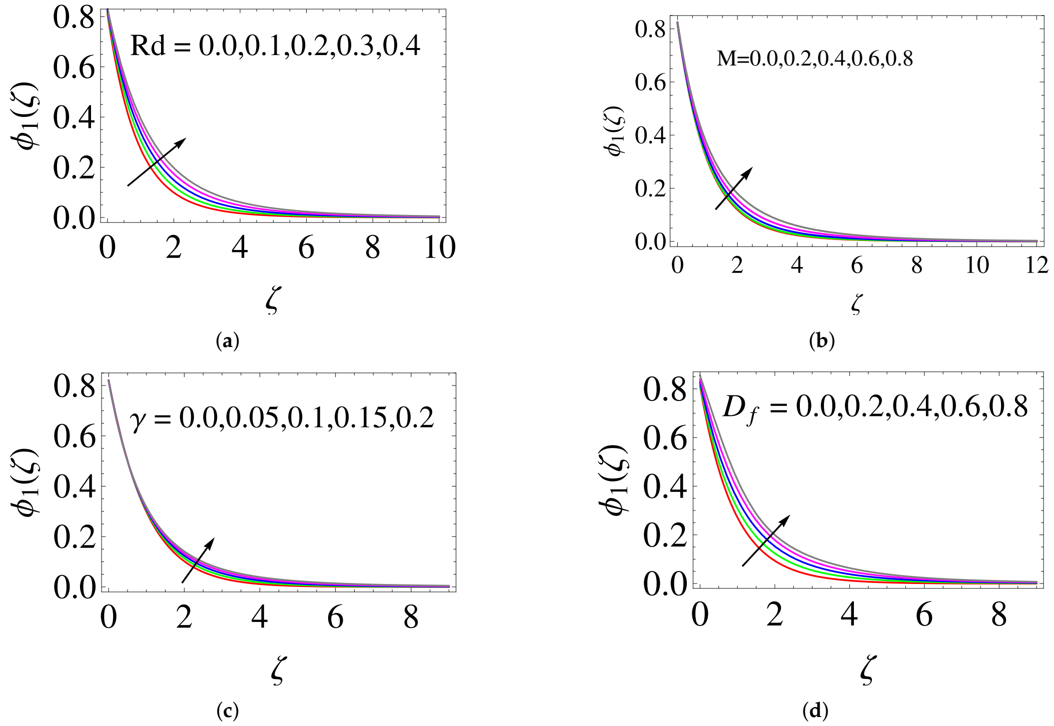

Figure 5. Influences of (**a**) thermal radiation (Rd), (**b**) magnetic (M), (**c**) curvature (γ) and (**d**) Dufour number (D_f) parameters on the temperature profile for $Nt = 0.1$, $\theta_w = 0.1$, $Nb = 0.1$, $Pr = 1.4$, $Sc_n = 1.9$, $Sc = 0.4$, $S_r = 0.2$, $C_r = 0.1$, $A = 0.1$, $G_1 = G_2 = G_3 = 0.1$ and $B_1 = B_2 = B_3 = 0.1$.

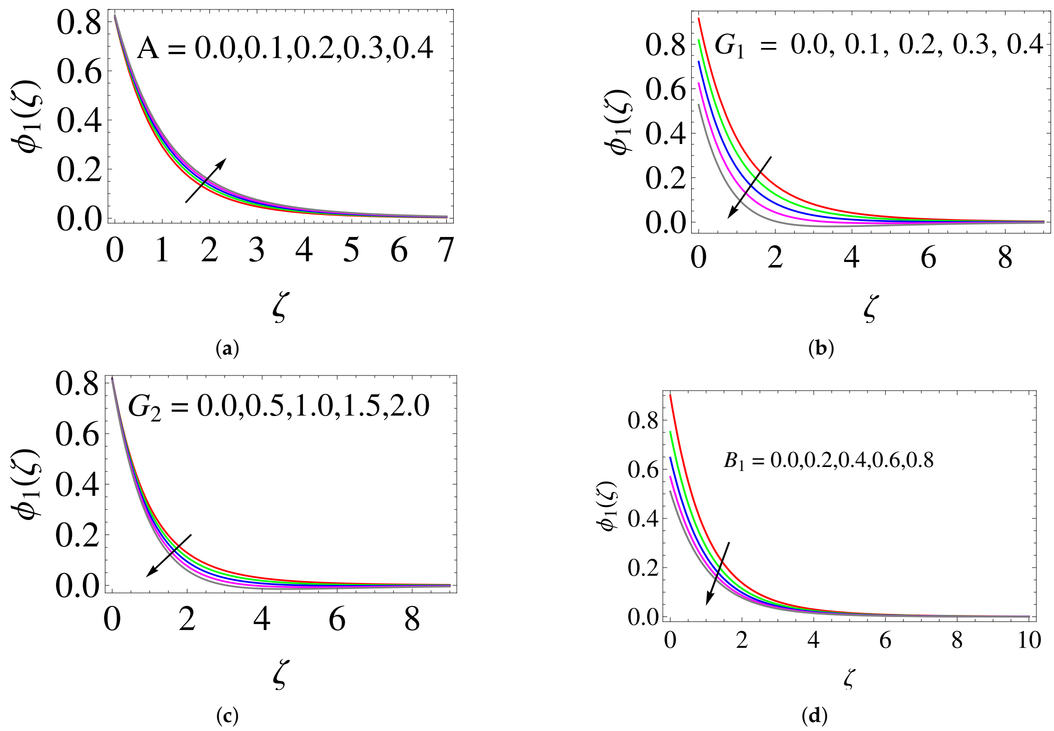

Figure 6. Influences of (**a**) velocity slip (A), (**b**) thermal stratification (G_1), (**c**) nanoparticle volume fraction stratification (G_2) and (**d**) thermal slip (B_1) parameters on temperature profile for $M = 0.2$, $Rd = 0.1$, $Nt = 0.1$, $\theta_w = 0.1$, $Nb = 0.1$, $Pr = 1.4$, $D_f = 0.2$, $Sc_n = 1.9$, $Sc = 0.4$, $S_r = 0.2$, $\gamma = 0.1$, $C_r = 0.1$, $G_3 = 0.1$ and $B_2 = B_3 = 0.1$.

It can be observed from Figure 7 that when magnetic parameter, curvature parameter, Dufour number and velocity slip factor are increased, the concentration profile increases. From Figure 8, it is clear that concentration profile diminishes if thermal stratification, concentration stratification parameter and concentration slip are increased.

It is clear from Figure 9 that the skin friction coefficient rises with enhancement in velocity slip factor. In Figures 10 and 11, the local Nusselt number decreases while increasing thermal radiation, Dufour number, thermal stratification and velocity slip factors. However, when the thermal slip factor is increased, it decreases for $0 \leq G_1 < 2.13$ and increases for $2.13 < G_1 \leq 4$. It remains unchanged (0.24) for different values of thermal slip factor when $G_1 = 2.13$. While increasing the NLTR and Dufour number, the local Sherwood number increases (see Figure 12), whereas it decreases while increasing the parameters Soret number, concentration stratification, concentration slip and velocity slip factor (see Figure 13).

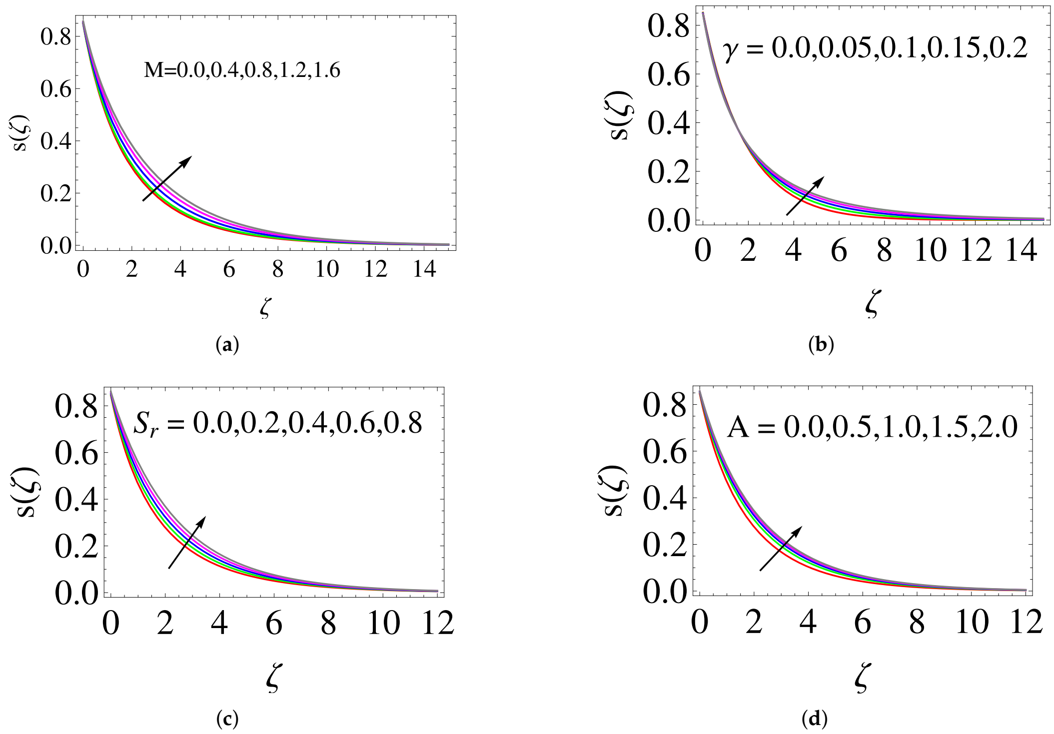

Figure 7. Influences of (**a**) magnetic (M), (**b**) curvature (γ), (**c**) Soret number (S_r) and (**d**) velocity slip (A) parameters on concentration profile for $Rd = 0.1$, $Nt = 0.1$, $\theta_w = 0.1$, $Nb = 0.1$, $Pr = 1.4$, $D_f = 0.2$, $Sc_n = 1.9$, $Sc = 0.4$, $C_r = 0.1$, $G_1 = G_2 = G_3 = 0.1$ and $B_1 = B_2 = B_3 = 0.1$.

The regression equation for skin friction with A, γ and M for 0.1, 0.2, 0.3, 0.4 and 0.5 are

$$Re_x^{1/2} C_f = -0.9149 + 0.7983 * A - 0.2942 * \gamma - 0.2598 * M. \tag{28}$$

The regression equation for local Nusselt number with A, B_1, B_2, D_f, G_1, G_2, γ, M and Rd for 0.1, 0.2, 0.3, 0.4 and 0.5 is

$$\begin{aligned} Re_x^{-1/2} Nu = 1.0397 - 0.2440 * A - 0.5730 * B_1 + 0.1084 * B_2 - 0.4534 * D_f \\ -0.2748 * G_1 + 0.0467 * G_2 + 0.1838 * \gamma - 0.0666 * M - 0.5210 * Rd. \end{aligned} \tag{29}$$

The regression equation for a local Sherwood number with A, B_1, B_2, B_3, C_r, D_f, G_1, G_2, G_3, γ, M, Rd and S_r for 0.1, 0.2, 0.3, 0.4 and 0.5 is

$$
\begin{aligned}
Re_x^{-1/2}Sh = {} & 0.5653 - 0.1131 * A + 0.0274 * B_1 - 0.0082 * B_2 - 0.2566 * B_3 \\
& +0.3382 * C_r + 0.0288 * D_f + 0.0032 * G_1 - 0.0036 * G_2 \\
& -0.3505 * G_3 + 0.3146 * \gamma - 0.0407 * M + 0.0325 * Rd - 0.1982 * S_r.
\end{aligned}
\tag{30}
$$

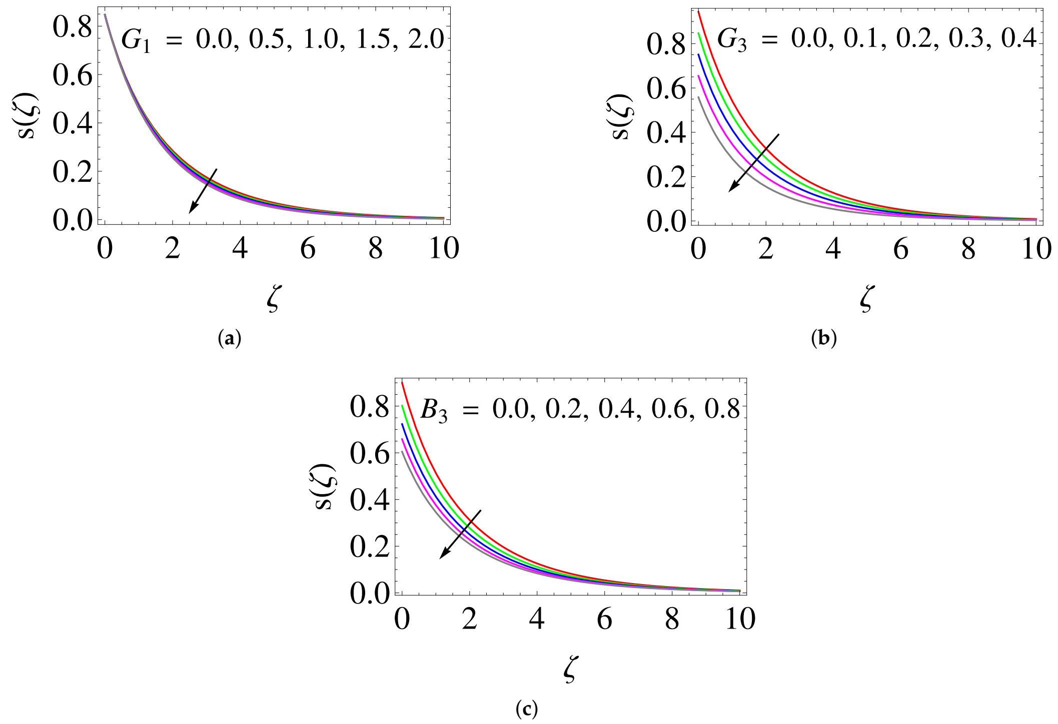

Figure 8. Influences of (**a**) thermal (G_1), (**b**) concentration (G_3) stratification and (**c**) concentration slip (B_3) parameters on concentration profile for $M = 0.2$, $Rd = 0.1$, $Nt = 0.1$, $\theta_w = 0.1$, $Nb = 0.1$, $Pr = 1.4$, $D_f = 0.2$, $Sc_n = 1.9$, $Sc = 0.4$, $S_r = 0.2$, $\gamma = 0.1$, $C_r = 0.1$, $A = 0.1$, $G_2 = 0.1$ and $B_2 = 0.1$.

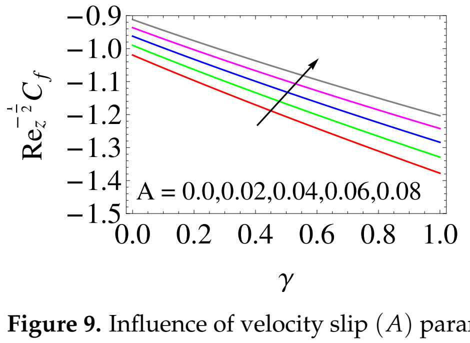

Figure 9. Influence of velocity slip (A) parameter on skin friction.

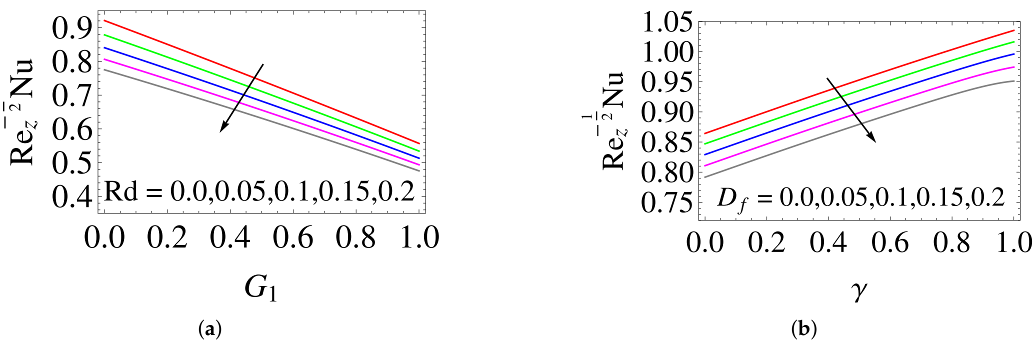

Figure 10. *Cont.*

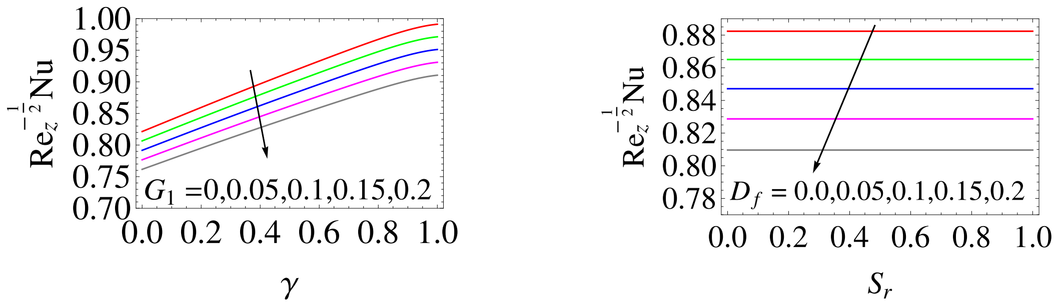

(**c**) (**d**)

Figure 10. Influences of (**a**) thermal radiation (Rd), (**b**,**d**) Dufour number (D_f) and (**c**) thermal stratification (G_1) parameters on Nusselt number.

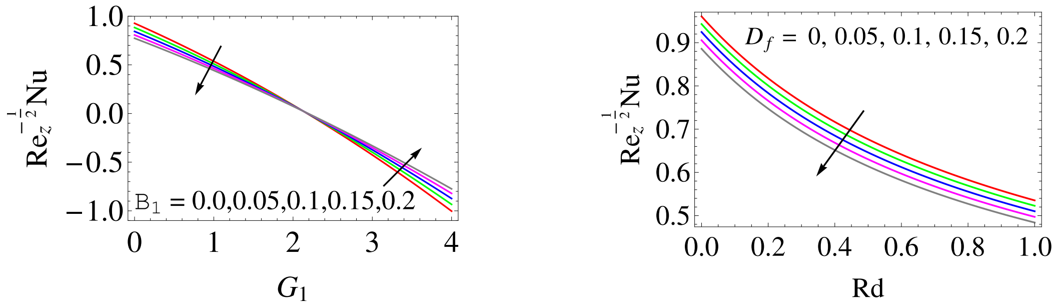

(**a**) (**b**)

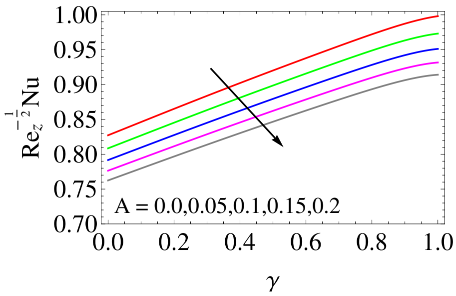

(**c**)

Figure 11. Influences of (**a**) thermal (B_1) slip, (**b**) Dufour number (D_f) and (**c**) velocity slip (A) parameters on Nusselt number.

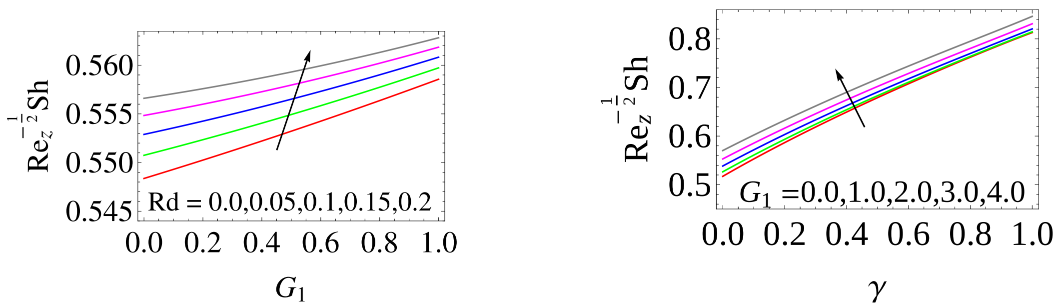

(**a**) (**b**)

Figure 12. *Cont.*

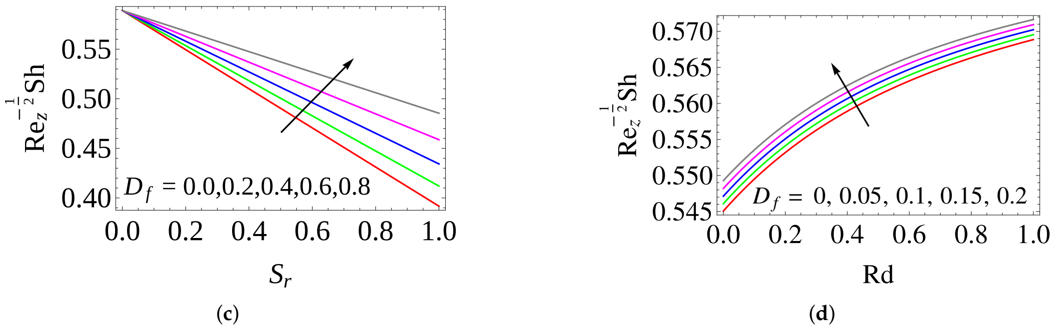

Figure 12. Influences of (**a**) thermal radiation (Rd), (**b**) thermal stratification (G_1) and (**c**,**d**) Dufour number (D_f) parameters on Sherwood number.

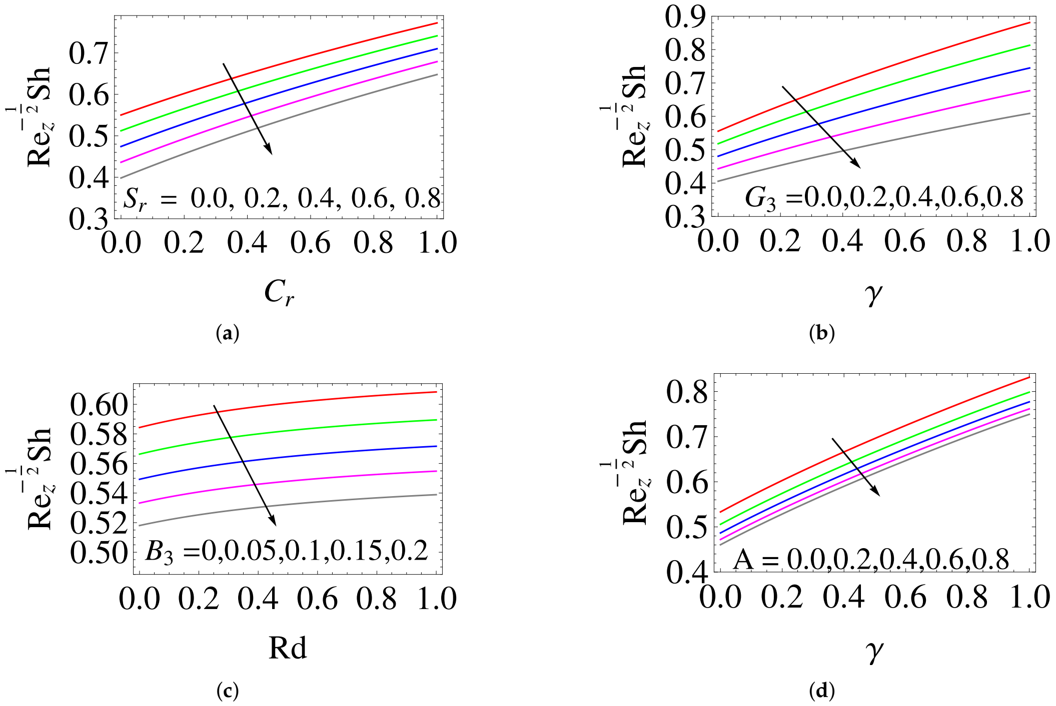

Figure 13. Influences of (**a**) Soret number (S_r), (**b**) concentration stratification (G_3), (**c**) thermal slip (B_3) and (**d**) velocity slip (A) parameters on Sherwood number.

5. Conclusions

The study of the impacts of slip, thermal radiation and Soret and Dufour on MHD nanofluid flow with TSF towards a stretching cylinder is offered. The main findings of this analysis are listed below as follows:

- While increasing the concentration slip, the solutal concentration boundary layer thickness shrinks, which results in a reduction in the rate of mass transfer.
- When the NLTR parameter value is increased, the local heat transfer rate reduces, whereas the local mass transfer rate increases.
- The thermal (concentration) boundary layer is thickened by increasing the Dufour (Soret) number.
- While raising thermal radiation, the thermal boundary layer thickness enhances.
- When the thermal energy, nanoparticle volume fraction and solutal stratification are increased, the thickness of thermal and solutal concentration boundary layers diminishes.

- The thermal and concentration boundary layer thickness and skin friction raise when the velocity slip is increased, whereas the momentum boundary layer thickness, heat and mass transfer rate diminish.
- The present results are very useful to the thermal science community to improve the cooling processes in heat transfer systems.

Author Contributions: Conceptualization, S.S.; methodology, K.J.; software, K.J.; validation, S.S. and K.J.; formal analysis, S.S. and K.J.; investigation, S.S. and K.J.; writing—original draft preparation, S.S. and K.J.; writing—review and editing, S.S. and K.J.; visualization, K.J.; supervision, S.S. All authors have read and agreed to the published version of the manuscript.

Funding: This research received no external funding.

Conflicts of Interest: The authors declare no conflict of interest.

Abbreviations

In this manuscript, the following abbreviations are used:

NLTR	Nonlinear thermal radiation
TSF	Triple stratification
MHD	Magneto-hydrodynamics
HAM	Homotopy analysis method

Nomenclature

c_p	specific heat ($J \cdot kg^{-1}$)
c_s	concentration susceptibility
k_T	thermal diffusion ratio
k_1	chemical reaction
l	reference length (m)
q_r	heat flux ($kg \cdot m^2 \cdot s^{-3}$)
u, w	r- and z-axis velocity components ($m \cdot s^{-1}$)
A	velocity slip parameter
B_0	strength of magnetic field ($m^{-1} \cdot A$)
B_1	thermal slip parameter
B_2	nanoparticles volume fraction slip parameter
B_3	concentration slip parameter
Cn	nanoparticles volume fraction
Cn_r	chemical reaction parameter
Cn_0	reference nanoparticles volume fraction
D_B	Brownian motion
D_f	Dufour (diffusion-thermo) number
D_s	mass diffusivity ($m^2 \cdot s^{-1}$)
D_{Te}	thermophoresis coefficient
G_1	thermal stratification parameter
G_2	nanoparticle volume fraction stratification parameter
G_3	concentration stratification parameter
K_1	thermal slip factor
K_2	nanoparticle volume fraction slip factor
K_3	concentration slip factor
L	magnetic parameter
Nb	Brownian motion parameter
Nt	thermophoresis parameter
Pr	Prandtl number
Rd	thermal radiation parameter
Re_z	local Reynolds number
S	concentration
Sc	Schmidt number
Sc_n	nanofluid Schmidt number

S_r	(thermal-diffusion) Soret number
S_0	reference concentration (m^{-3}·mol)
Te	temperature (K)
Te_m	mean fluid temperature
Te_0	reference temperature
W_0	uniform velocity of the plate
Greek Symbols	
α	thermal diffusivity (m^2·s^{-1})
γ	curvature parameter
ν	kinematic viscosity of the fluid (m^2·s^{-1})
ρ	density of the fluid (kg·m^{-3})
τ	ratio between the effective nanoparticles materials and fluid heat capacity
θ_w	temperature ratio parameter
σ	electrical conductivity (S·m^{-1})

References

1. Rahman, M.M.; Aziz, A. Heat transfer in water based nanofluids (TiO_2–H_2O, Al_2O_3–H_2O and Cu–H_2O) over a stretching cylinder. *Int. J. Heat Mass Transf.* **2012**, *30*, 31–42. [CrossRef]
2. Rasekh, A.; Ganji, D.D.; Tavakoli, S. Numerical Solutions for a Nanofluid Past over a Stretching Circular Cylinder with Non-Uniform Heat Source. *Front. Heat Mass Transf.* **2012**, *3*, 043003. [CrossRef]
3. Pandey, A.K.; Kumar M. Natural convection and thermal radiation influence on nanofluid flow over a stretching cylinder in a porous medium with viscous dissipation. *Alex. Eng. J.* **2017**, *56*, 55–62. [CrossRef]
4. Das, M.; Mahatha, B.K.; Nandkeolyar R. Mixed Convection and Nonlinear Radiation in the Stagnation Point Nanofluid flow towards a Stretching Sheet with Homogenous-Heterogeneous Reactions effects. *Procedia Eng.* **2015**, *127*, 1018–1025. [CrossRef]
5. Raju, C.S.K.; Sandeep, N.; Gnaneswara Reddy, M. Effect of Nonlinear Thermal Radiation on 3D Jeffrey Fluid Flow in the Presence of Homogeneous–Heterogeneous Reactions. *Int. J. Eng. Res. Afr.* **2015**, *21*, 52–68. [CrossRef]
6. Abbas, Z.; Perveen, R.; Sheikh, M.; Pop, I. Thermophoretic diffusion and nonlinear radiative heat transfer due to a contracting cylinder in a nanofluid with generalized slip condition. *Results Phys.* **2016**, *6*, 1080–1087. [CrossRef]
7. Uddin, M.J.; Rana, P.; Anwar Bég, O.; Ismail, A.I.M. Finite element simulation of magnetohydrodynamic convective nanofluid slip flow in porous media with nonlinear radiation. *Alex. Eng. J.* **2016**, *55*, 1305–1319. [CrossRef]
8. Kumar, M.S.; Sandeep, N.; Kumar, B.R.; Prakash, J. Effect of Cattaneo–Christov Heat Flux on Nonlinear Radiative Mhd Flow of Casson Fluid Induced by a Semi-Infinte Stretching Surface. *Front. Heat Mass Transf.* **2017**, *8*, 8.
9. Veera Krishna, M.; Chamkha, A.J. Hall and ion slip effects on Unsteady MHD Convective Rotating flow of Nanofluids—Application in Biomedical Engineering. *J. Egypt. Math. Soc.* **2020**, *28*, 1–15. [CrossRef]
10. Veera Krishna, M. Hall and ion slip effects on radiative MHD rotating flow of Jeffreys fluid past an infinite vertical flat porous surface with ramped wall velocity and temperature. *Int. Commun. Heat Mass Transf.* **2021**, *126*,105399. [CrossRef]
11. Veera Krishna, M.; Chamkha, A.J. Hall and ion slip effects on MHD Rotating Boundary layer flow of Nanofluid past an infinite vertical plate Embedded in a Porous medium. *Results Phys.* **2019**, *15*, 102652. [CrossRef]
12. Animasaun, I.L.; Ibraheem, R.O.; Mahanthesh, B.; Babatunde, H.A. A meta-analysis on the effects of haphazard motion of tiny/nano-sized particles on the dynamics and other physical properties of some fluids. *Chin. J. Phys.* **2019**, *60*, 676–687. [CrossRef]
13. Chamkha, A.J.; Abd El-Aziz, M.M.; Ahmed, S.E. Effects of thermal stratification on flow and heat transfer due to a stretching cylinder with uniform suction/injection. *Int. J. Energy Technol.* **2010**, *2*, 1–7.
14. Mukhopadhyay, S.; Ishak, A. Mixed Convection Flow along a Stretching Cylinder in a Thermally Stratified Medium. *J. Appl. Math.* **2012**, *2012*, 491695. [CrossRef]
15. Karthikeyan, S.; Bhuvaneswari, M.; Sivasankaran, S.; Rajan, S. Soret and Dufour effects on MHD mixed convection heat and mass transfer of a stagnation point flow towards a vertical plate in a porous medium with chemical reaction, radiation and heat generation. *J. Appl. Fluid Mech.* **2016**, *9*, 1447–1455. [CrossRef]
16. Eswaramoorthi, S.; Bhuvaneswari, M.; Sivasankaran S.; Rajan, S. Soret and Dufour effects on viscoelastic boundary layer flow over a stretching surface with convective boundary condition with radiation and chemical reaction. *Sci. Iran. B* **2016**, *23*, 2575–2586. [CrossRef]
17. Hayat, T.; Nassem, A.; Khan, M.J.; Farooq, M.; Al-Saedi, A. Magnetohydrodynamic (MHD) flow of nanofluid with double stratification and slip conditions. *Phys. Chem. Liq.* **2018**, *56*, 189–208. [CrossRef]
18. Faraz, F.; Imran, S.M.; Ali, B.; Haider, S. Thermo-Diffusion and Multi-Slip Effect on an Axisymmetric Casson Flow over a Unsteady Radially Stretching Sheet in the Presence of Chemical Reaction. *Processes* **2019**, *7*, 851. [CrossRef]
19. Ali, B.; Naqvi, R.A.; Haider, A.; Hussain, D.; Hussain, S. Finite Element Study of MHD Impacts on the Rotating Flow of Casson Nanofluid with the Double Diffusion Cattaneo–Christov Heat Flux Model. *Mathematics* **2020**, *8*, 1555. [CrossRef]
20. Abdal, S.; Mariam, A.; Ali, B.; Younas, S.; Ali, L.; Habib, D. Implications of bioconvection and activation energy on Reiner–Rivlin nanofluid transportation over a disk in rotation with partial slip. *Chin. J. Phys.* **2021**, *73*, 672–683. [CrossRef]

21. Noor, N.F.M.; Haq, R.U.; Abbasbandy, S.; Hashim, I. Heat flux performance in a porous medium embedded Maxwell fluid flow over a vertically stretched plate due to heat absorption. *J. Nonlinear Sci. Appl.* **2016**, *9*, 2986–3001. [CrossRef]
22. Noor, N.F.M.; Hashim, I. Thermocapillarity and magnetic field effects in a thin liquid film on an unsteady stretching surface. *Int. J. Heat Mass Transf.* **2010**, *53*, 2044–2051. [CrossRef]
23. Andersson, H. Slip flow past a stretching surface. *Acta Mech.* **2002**, *158*, 121–125. [CrossRef]
24. Mahmoud, M.A. Chemical reaction and variable viscosity effects on flow and mass transfer of a non-Newtonian visco-elastic fluid past a stretching surface embedded in a porous medium. *Meccanica* **2010**, *45*, 835–846. [CrossRef]
25. Mahmoud, M.A.; Waheed, S.E. MHD flow and heat transfer of a micropolar fluid over a stretching surface with heat generation (absorption) and slip velocity. *J. Egypt Math Soc.* **2012**, *20*, 20–27. [CrossRef]